Pergamon

*Transpn Res.-D.* Vol. 3, No. 3, pp. 171–191, 1998

Printed in Great Britain
1361-9209/98 $19.00 + 0.00

PII: S1361-9209(97)00029-1

# A MATHEMATICAL MODEL OF WIND FLOW, VEHICLE WAKE, AND POLLUTANT CONCENTRATION IN URBAN ROAD MICROENVIRONMENTS. PART II: MODEL RESULTS

MD. MASUD KARIM*†
Dainichi Consultant Inc., 3-1-21 Yabuta Minami, Gifu 500, Japan

HIROSHI MATSUI
Department of Civil Engineering, Nagoya Institute of Technology, Gokiso-cho, Showa-ku, Nagoya 466, Japan

and

RANDALL GUENSLER
School of Civil and Environmental Engineering, Georgia Institute of Technology, Atlanta, GA 30332-0355, U.S.A.

*(Received 19 May 1997; accepted 12 October 1997)*

**Abstract**—Theoretical formulations of the proposed model for prediction of pollutant dispersion in micro-environments was previously introduced in part I of this paper (Karim and Matsui, 1998). This paper discusses the new model findings and presents model evaluation results. This paper first explains the current problems that the road environment plays in employing field data for wind and temperature collected along a road north of Nagoya, Japan. A complete simulation is done on wind components in street-canyon and wind distribution, including vehicle wake effect, and is evaluated with experimental results. Next, the paper provides the atmospheric stability and dispersion parameters and then predicts pollutant buildups estimated using several techniques: a numerical model, modified Gaussian dispersion model, and a stochastic model. The stochastic model is specially developed to predict pollutant buildups in microenvironments. Model sensitivity analysis is done, varying the physical parameters; vehicle dimensions to wind speed in microenvironments, vehicle dimensions to dispersion parameter, and wind speed to pollutant concentrations. The modeled results are then compared to experimental data collected in micro-environmental locations in a road of Nagoya City, Japan. Finally, the implications of the research findings are discussed. © 1998 Elsevier Science Ltd. All rights reserved

*Keywords*: traffic pollution, road microenvironments, pollutant buildup, sensitivity analysis

## 1. INTRODUCTION

Part I of this paper (Karim and Matsui, 1998) presented a detailed description of a model that predicts wind speed, pollutant dispersion and buildups in urban road microenvironments. Part II concentrates on the important findings and model results. The application of the proposed model produced some interesting findings and revealed relationships, some of which have already been discussed in our previous publications (Karim and Matsui, 1995; Karim, 1997, chap. 5 and 6) and will be outlined only briefly in Section 6. In this paper, we will, however, emphasize the sensitivity analysis of the various model parameters and the prediction of microenvironmental pollutant buildups.

The structure of this paper is therefore organized as follows. Section 2 gives details of the experimental setup and computer aspects. Section 3 summarizes emission and pollutant concentration trends, Section 4 provides atmospheric stability and dispersion parameters due to three physical factors; ambient turbulence, vehicle-induced turbulence, and thermal turbulence. Section 5 outlines pollution prediction in microenvironments. Section 6 presents model sensitivity varying model parameters and finally in Section 7 the evaluation of the model and conclusions are made based on the results of the model.

*Author for correspondence.
†Work done while Ph.D. student at Nagoya Institute of Technology, Nagoya, Japan.

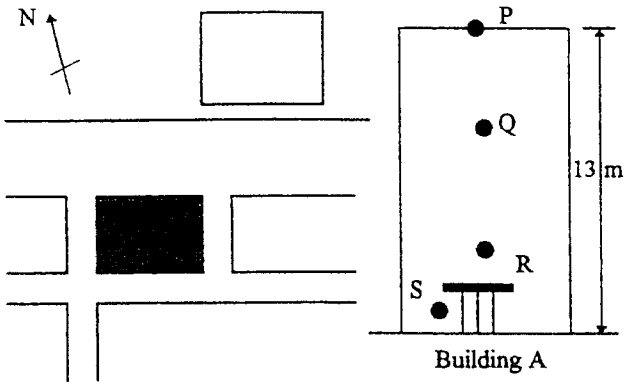


Fig. 1. Geometry of experimental road.

## 2. EXPERIMENTAL SETUP AND COMPUTER ASPECTS OF THE MODEL

The experimental setup for pollutant concentration monitoring and meteorological data was done in the north of Nagoya City. Nagoya City has 26 monitoring stations regularly monitoring pollutant data. The geometry of the experimental site is presented in Fig. 1. The fixed sensors are located at points P, Q, and R in Fig. 1. The points are at heights of 13, 8, and 2.3 m, respectively, and the height of the road level receptor (point S, especially designed for our experimental setup) is located at 1 m from the ground. At point P, hourly average wind speed, wind direction, and temperature; at point Q, hourly average concentrations for NO, $NO_2$, and $NO_x$; at point R, hourly average concentration of CO; and at point S, wind speed, temperature, concentration of NO, $NO_2$, and $NO_x$ data are monitored.

A northeast co-ordinate system (Fig. 2) is used in the computer model. The co-ordinates (a, b) of any point along the line at an arbitrary distance, $r$ (m), from point A are given by:

$$a = a_A + r \sin \beta \tag{1}$$

$$b = b_A + r \sin \beta \tag{2}$$

Given a receptor at $(a_k, b_k)$ the downwind distance $x$ (m), and the crosswind distance $y$ (m), of the receptor from the point (a, b) for any wind direction $\alpha$ (degrees) are given by:

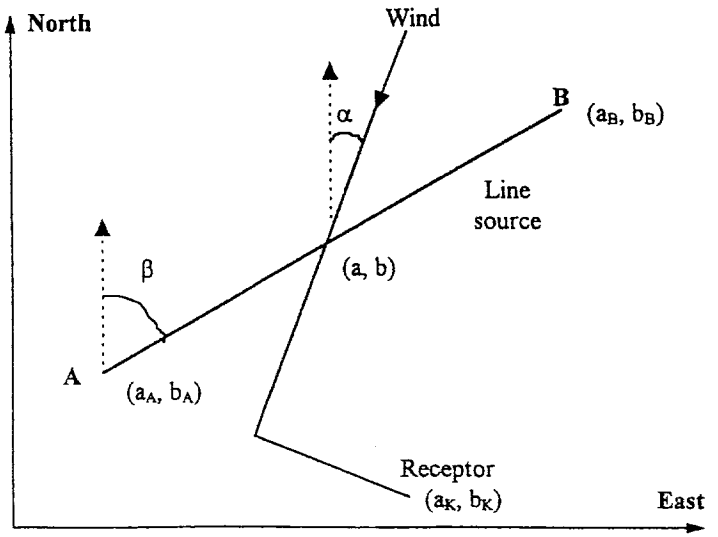


Fig. 2. Line source and receptor relationships.

$$x = (b - b_k)\cos\ \alpha + (a - a_k)\ \sin\ \alpha \tag{3}$$

$$y = (b - b_k)\ \sin\ \alpha - (a - a_k)\ \cos\ \alpha \tag{4}$$

The width of the highway and canyon, height of the building, width of footpath, vehicle dimensions, positions of the vehicles on the road, and coordinates of the receptors are the input parameters. However, in eqns (3) and (4), $x$ and $y$ refer to a co-ordinate system aligned along the wind vector ($x$, the downwind direction, and $y$, the upwind direction). This system is totally different from the co-ordinate system used for locating sources and receptors in the model.

The BASIC computer program consists of a main routine and nine sub-routines. Figure 3 depicts the general flow of the model. The main routine handles memory allocation for the variables and defines the steps of sub-routine jobs to perform. Sub-routine READ.DATA reads model parameter for the particular location to run the model. In reading input data from file sub-routine READ.FILE is used. Sub-routine SAVE.DATA does the saving and printing of all output results in files. The sub-routine calls EMISSION.RATE, which estimates the rate of emission or source strength in g $m^{-1}$ $s^{-1}$. Sub-routine WIND.SPEED manipulates wind data, estimates wind components in street canyon, and wind speed fluctuations in the wake of vehicles in street canyon. Evaluation of dispersion parameters is done by sub-routine TURBULENCE that estimates the tailpipe emission concentration. Sub-routine GAUSS.DISTRIBUTION evaluates modified Gaussian equations to estimate active pollutant concentrations. The sub-routine STATISTICS outline the multivariate normal probability density functions and sub-routine STOCH does the

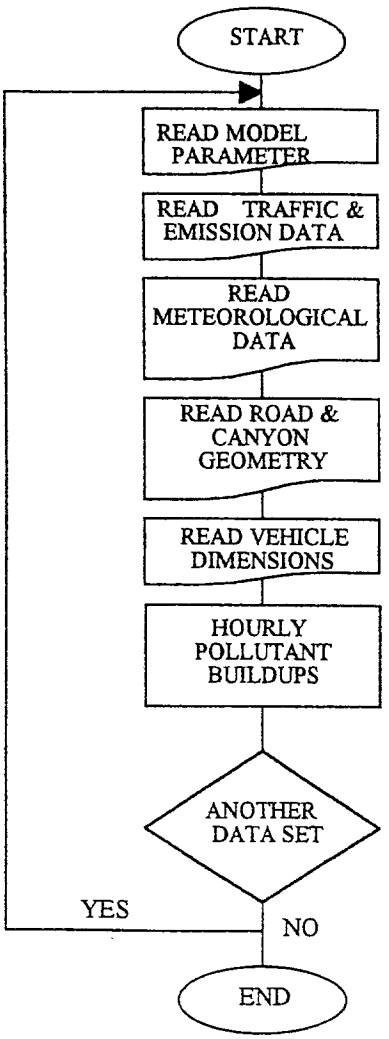


Fig. 3. General flow diagram for the model.

numerical integration to calculate the probability to predict the buildup of pollutants concentration in microenvironments. The program is capable of processing multiple hours of meteorology with a wide variety of fleet composition.

## 3. EMISSION AND POLLUTANT CONCENTRATION TRENDS

### *3.1. Traffic flow and resulting emission*

Traffic flow and resulting emissions are the primary physical attributes for polluting urban roads. Traffic flow and emission rate are taken together to calculate source strength. The model uses traffic flow data for the emission rate calculation process. Traffic flow census data were available for weekdays from 7 a.m. to 6 p.m. Weekday and weekend traffic flows vary substantially in urban areas. There are eight major categories of Japanese vehicles and the rate of emission from each category is estimated as a function of running speed and fuel categories. For calculation ease, eight polynomials represent the categories of vehicle emissions (Karim and Matsui, 1994). Some subfleet composition effects were included through the assumption of technology distributions.

For example, total bus traffic was assumed to be represented by; 10% gasoline-powered microbus, 20% diesel-powered microbus, 10% gasoline-powered heavy-bus, and 60% diesel-powered heavy-bus.

Figures 4 and 5 represent traffic flows and resulting emissions at different hours of a day. Figure 4 represents $NO_x$ emission with traffic flows. $NO_x$ emission follows the trends of traffic flows on road. At 11:00, 12:00, and 13:00 h $NO_x$ emission violate the standard trends. At 11:00 and 13:00 h the number of heavy duty vehicles are less compared to light duty vehicles, which results in inverse relationship to traffic flows. And at 12 noon, the number of heavy-duty vehicles are larger than the light duty vehicles (LDV). Figure 5 presents CO emission with daily traffic flows. It is observed that CO emission is greater from light duty vehicles during lower average speed. Two important parameters that determine the level of CO emissions from LDVs, LDTs, and motorcycles are ambient temperature and the numbers of these vehicles.

### *3.2. Ambient concentration*

The Japanese ambient concentration standard for nitrogen dioxide ($NO_2$) requires a daily average of hourly values to remain below 0.06 parts per million (ppm). In an area where the daily average of hourly values exceeds 0.06 ppm, efforts should be made to achieve the 0.06 ppm level. In an area where the daily average of hourly values falls within the range of 0.04–0.06 ppm, efforts should be made so that the ambient concentrations are maintained around the present level. The standard for CO requires concentrations to remain below 10 ppm, expressed as a daily average hourly value.

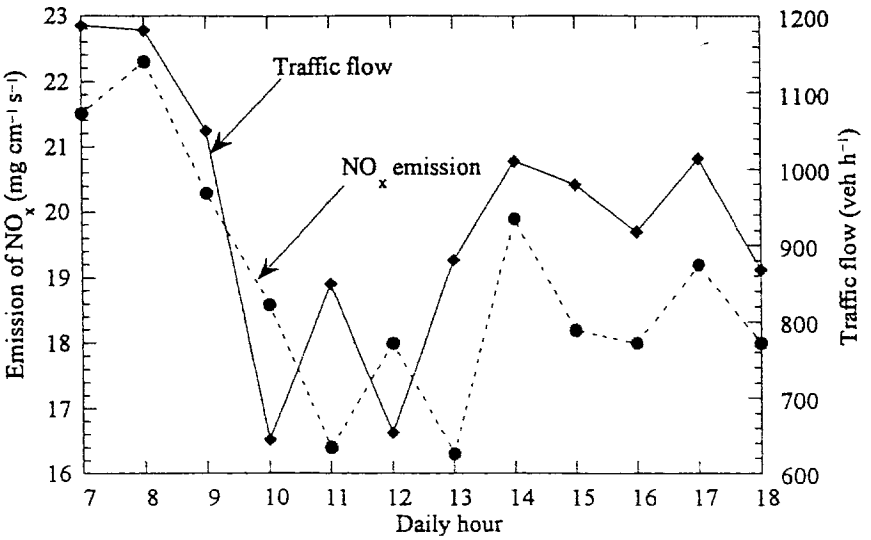


Fig. 4. Traffic flows and $NO_x$ emissions.

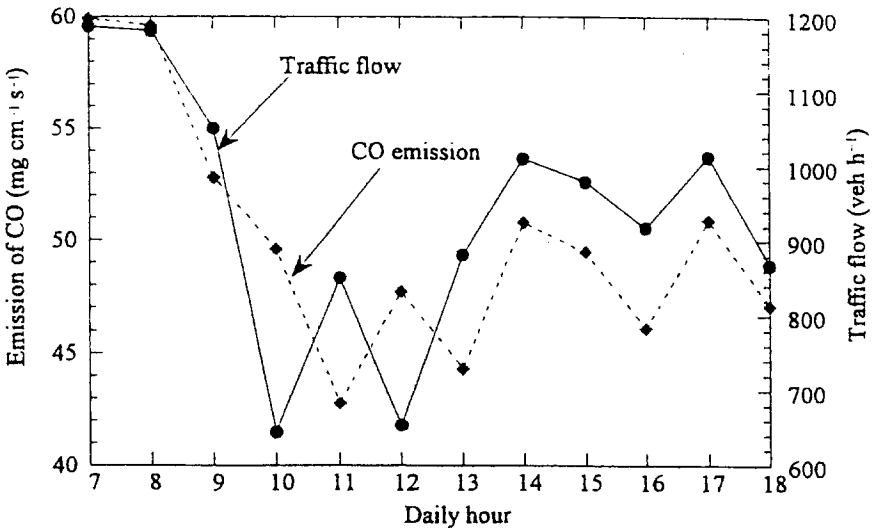


Fig. 5. Traffic flows and CO emissions.

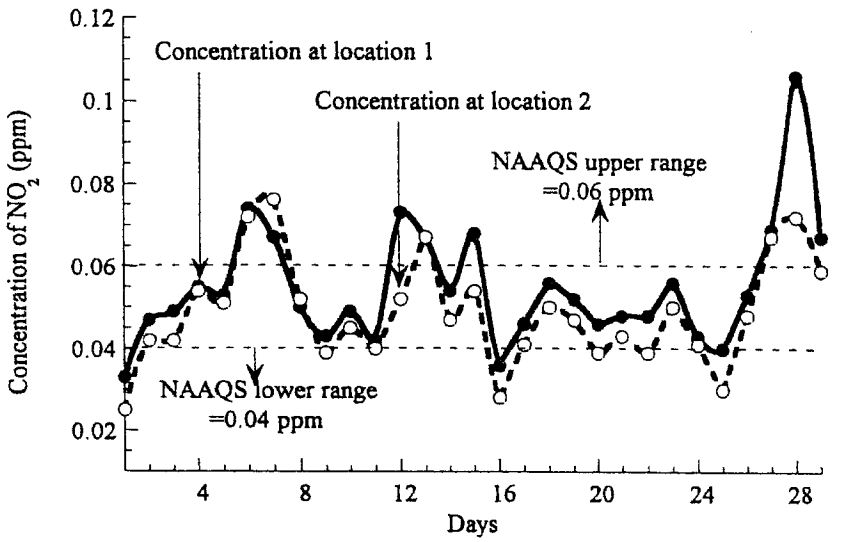


Fig. 6. Daily average $NO_2$ concentrations near two roads in Nagoya City, Japan.

Figures 6 and 7 present the hourly concentration trends for $NO_2$ and CO at two fixed monitoring stations in Nagoya. Exhaust emissions from internal combustion engines result in severe air pollution that exceeds regulatory standards for $NO_2$ in Nagoya City, Japan. In Fig. 6, it is clear that $NO_2$ concentrations fall within the concentration range of concern and sometimes exceed the 0.06 ppm $NO_2$ standard. The CO trends appear to fall within acceptable limits.

### *3.3. Wind speed and pollutant concentrations*

Wind speed determines the extent to which pollutants are initially diluted with ambient air at the point of release. This effect is treated as an inverse relationship between wind speed and concentration in the Gaussian formula. Figures 8–10 present the relationships between ambient wind and CO, NO, and $NO_2$ concentrations. Wind speed also plays an important role in the dispersion parameter computations. It determines the wind velocity fluctuations in the wake of vehicles, is used for computing the lateral and vertical dispersion parameter due to vehicle induced turbulence, and is also involved in the stability calculation and heat flux modifications to the vertical dispersion curve. It is also used in horizontal and vertical dispersion parameter computations for ambient turbulence. Maximum concentrations occur under lower ambient wind, which can be clearly observed in the figures.

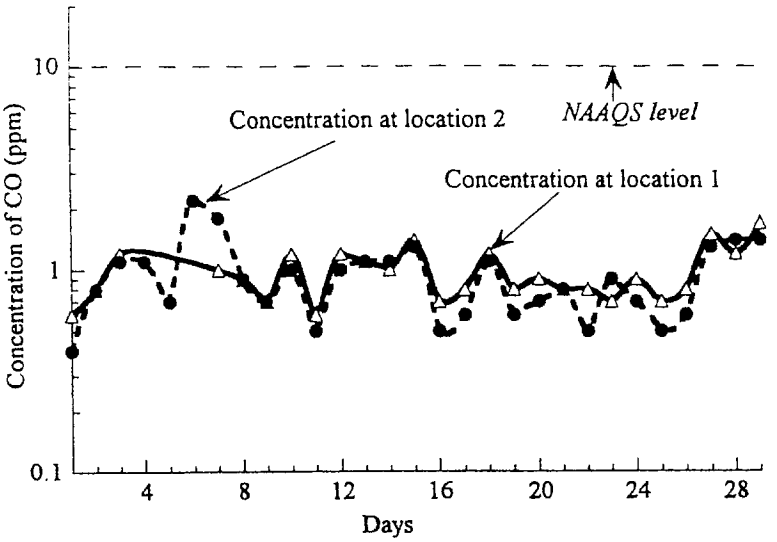


Fig. 7. Daily average CO concentrations near two roads in Nagoya City, Japan.

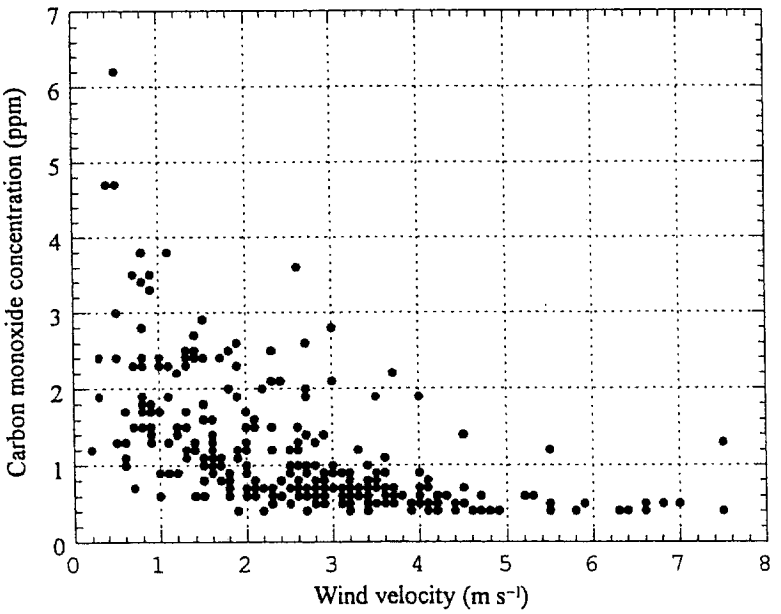


Fig. 8. Ambient wind and CO concentrations.

The wind direction is important in determining the orientation of the pollutant plume and therefore the concentration at a particular location outside of the mixing zone, wind angle, $\alpha = 10°$ yields the highest concentration (Benson, 1989). A smooth buildup of concentration across the mixing zone is readily apparent in the $\alpha = 90°$, in ground level case ($z = 0$). Maximum concentration occurs normally under near-perpendicular wind conditions for all wind speeds. This maximum becomes less pronounced at higher wind speeds and greater distances. The wind-road angles at peak concentration appear to be relatively independent of wind speed, and to shift slightly away from parallel at greater receptor distances.

## 4. ATMOSPHERIC STABILITY AND DISPERSION PARAMETERS

Transport and dispersion are the most complicated processes in air quality modeling and are solved in stochastic manner. The exact solution to represent real-world-complexities is still unresolved. Gaussian solutions for dispersion have been assumed. In most dispersion models, six

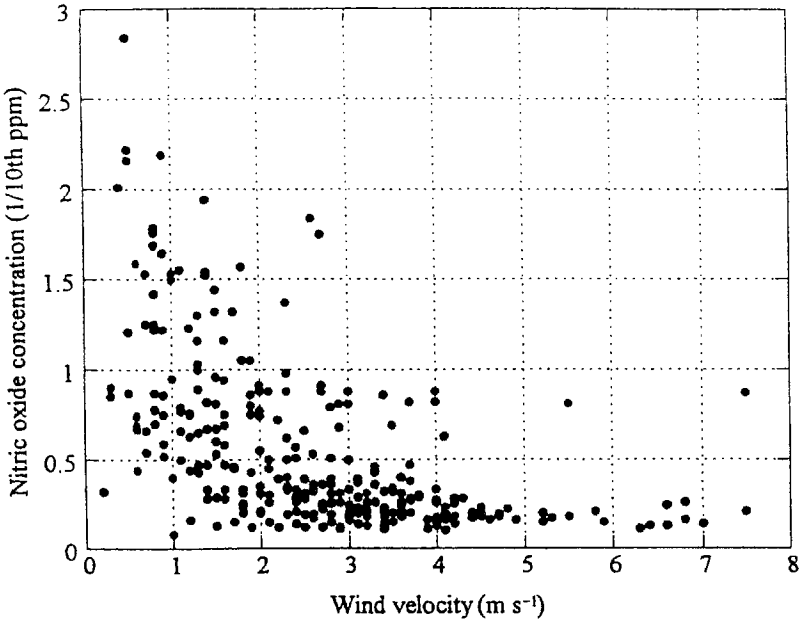


Fig. 9. Ambient wind and $NO_x$ concentrations.

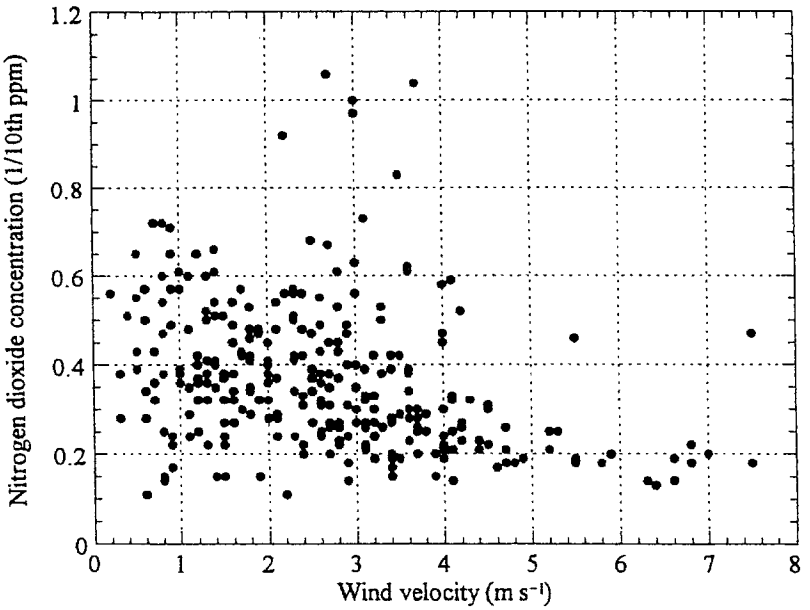


Fig. 10. Ambient wind and $NO_2$ concentrations.

classes of stability are based upon Pasquil–Gifford (PG) curves. However, PG curves were originally established for downwind distances beginning at 100 m from a point source and do not necessarily provide a reliable description of near field dispersion. Instead, a mathematical representation of stability (Chock, 1978), based on the numerical values of Richardson's number, is employed in the new model. In this method, only three categories of stability are employed to represent microscale atmospheric conditions: stable, unstable, and neutral. In the real world, atmospheric conditions are changing at every moment, so the proposed established conditions are merely an approximation of a natural process.

The measured and calculated wind and temperature data at various levels of the urban street canyon are employed to estimate Richardson's number for one hour average conditions.

Transport and dispersion cause the motion of pollutants in the atmosphere. Transport is a movement due to airflow. The movement (advection) of air across the surface of the earth can

occur in one of two distinct modes: laminar and turbulent flow. In the atmosphere, transport of an air mass is almost always turbulent. Violent swirling motions characterize turbulent flow and the presence of eddies.

Dispersion is the separation of pollutants within an air flow, resulting from ambient turbulence, turbulence induced by automobiles, and heat generated from vehicles. For a system of pollutant sources and receptors, models are used to predict downwind pollutant concentrations, based upon dispersion parameters. Using previously collected field data, dispersion relationships in established models (Eskridge and Hunt, 1979; Yamartino and Wiegand, 1986) are simplified and employed in the new model. The restructured dispersion parameters are described in detail in part I (Karim and Matsui, 1998) of this paper.

Dispersion parameters summarize the effects of vehicle induced turbulence, ambient turbulence, and heat flux. Hence, dispersion parameters due to ambient turbulence and thermal turbulence are developed for each stability class, wind direction, road-canyon geometry, and traffic flows, and dispersion due to vehicle wake turbulence is estimated for different modal split, vehicle dimensions, physical properties of the atmosphere, and boundary layer obstacles. Though gas particles have turbulent motion, prediction of the transport for pollutant is simplified by assuming dispersion in a conic volume in the near vicinity of the source. For the computation of dispersion parameter:

- reference height, $z_r = 13.0$ m
- surface roughness, $z_o = 0.4$ m
- constant, $\nu = 0.4$
- absolute temperature, $\theta = 273\,^{\circ}\mathrm{K}$
- drag coefficient, $C_D = 0.52$
- air density, $\rho = 1.225$ kg m$^{-3}$
- acceleration due to gravity, $g = 9.8$ m s$^{-2}$
- downwind distance, $l = 0.0073$ km
- canyon width, $B = 30.0$ m
- dispersion width in excess of road width, $b = 1.5$ m, and
- traffic flow per second ($N_a$) for each individual hour.

Table 1 presents vehicle dimensions of eight different categories of Japanese vehicles. This research considers vehicular dimensions in calculating dispersion parameter due to vehicle induced turbulence.

Vertical dispersion due to wake turbulence generated by traffic is a function of the cross-road wind component. For higher wind speeds, vehicle turbulence impact on dispersion is considered to be constant. For a cross-road wind speed greater than 3.91 m s$^{-1}$, vertical dispersion due to traffic induced turbulence is estimated to be 1.5 m (Petersen, 1980). Under low cross-road wind conditions, ambient turbulence and thermal turbulence can cause dispersion. The dispersion due to heat flux takes into account the total effects of solar radiation and vehicle-generated heat. Heat loss from different categories of vehicles are definitely different, but an average value of 0.8187 kW m$^{-1}$ has been taken for a fuel economy of 25.5 km l$^{-1}$ (60 mpg) and is employed in the model estimation.

## 5. PREDICTION FOR MICROENVIRONMENTAL POLLUTION

Pollution dispersion is a continuous process. For predicting pollution in microenvironments, multivariate normal probability density functions are employed. Pollutant concentrations and

Table 1. Average dimensions of Japanese vehicles

| Vehicle types | Height (m) | Width (m) | Length (m) |
|---|---|---|---|
| Passenger car ( < 660 cc) | 1.44 | 1.395 | 3.295 |
| Passenger car ( > 660 cc) | 1.375 | 1.735 | 4.6 |
| Bus | 3.112 | 2.309 | 9.216 |
| Truck ( < 660 cc) | 1.79 | 1.395 | 3.285 |
| Truck > 660 cc < 2000 cc | 2.041 | 1.834 | 4.867 |
| Van | 1.854 | 1.578 | 3.969 |
| Truck > 4 t | 2.902 | 2.458 | 10.726 |
| Special types | 2.793 | 2.602 | 6.861 |

wind speed are continuous variables. Probability density function of these continuous random variables follow bivariate normal probability distribution. To estimate the maximum concentration at the exposure level, multivariate continuous probability density functions (Lloyd, 1980; Tong, 1990) are used. Numerical integration of the density function prediction is performed to estimate probability for computed wind speed and tailpipe pollutant concentration. Exercising probability values, concentration near the ground were calculated from corresponding field data at the appropriate height. Predicted concentrations are defined as the active pollutants emitted directly from vehicle tailpipes at any event, plus pollutants from the previous event that have not been transferred out of the canyon (the background concentration).

Hourly pollutant concentrations and wind speed values collected under similar traffic conditions are first assembled. Probability distribution functions are then developed from a data set of 1440 measurements (288 for each of $NO_x$, NO, $NO_2$, and CO and 288 for wind speed). Figures 11 and 12 are the graphical representations of the density function distributions.

Figures 13 and 14 provide the model-predicted hourly concentrations near ground and at the mounted receptor site for $NO_x$ and CO, respectively. The variation of traffic flows and wind speed with corresponding hours are also shown in Figs 13 and 14. Peak points of the pollutant concentrations in Figs 13 and 14 follow the peak traffic hours (from 7 to 9 a.m. and from 6 to 8 p.m.) on Japan's roads. Traffic flows for these periods on our experimental road (three lanes) are 1187, 1181, 1050, and 1013 veh $h^{-1}$. In the morning, maximum traffic flow occurs at 7 a.m. and peak point of concentration appears likely between 8 and 9 a.m.

Wind speed substantially dominates the dispersion process. At 7 and 8 a.m., wind velocities are very low resulting in inadequate dispersion and hence higher concentration levels. If we examine the wind distribution, the periods of higher concentrations correspond to very mild wind velocities, around 1 to 2 m $s^{-1}$. When wind speeds are higher, in the periods from 2 to 4 p.m., concentrations are lower. Strong winds reduce the buildup of pollutants along the road. As expected, worst case situations occur under conditions of low wind speeds. The time lag between the concentration peaks are due to inadequate instantaneous dispersion (i.e. pollutant during the previous moments cannot be sufficiently transferred to the surroundings and upper air levels). Deficient transport, caused by the street canyon's hindrance of pollutant movement, contributes to a buildup of pollutants in the street canyon.

Figures 13 and 14 indicate that there are marked differences between predicted roadside concentration and monitored concentrations at elevated monitoring stations. When wind velocity is less than 1.5 m $s^{-1}$ the ratios between Computed Roadside Concentration (CRC) and Concentration at Mounted Receptor (CMR) are around 22 for $NO_x$ and 6 for CO. For wind speeds from 1.5 to 2 m $s^{-1}$, the CRC/CMR values are around 9 for $NO_x$ and 3 for CO. For wind velocities between 2 and 2.5 m $s^{-1}$, the ratios are 7 and 2.5 for $NO_x$ and CO, respectively. For wind velocities between

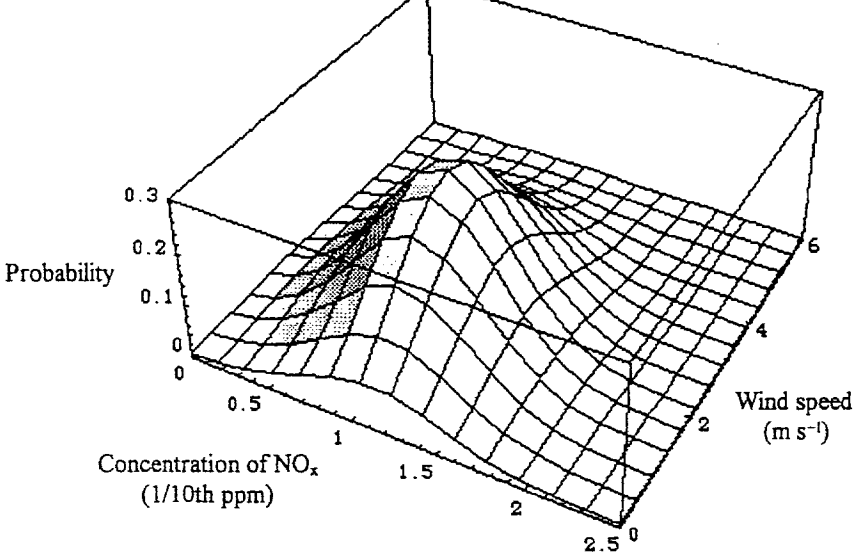


Fig. 11. Computed continuous normal probability distribution for $NO_x$.

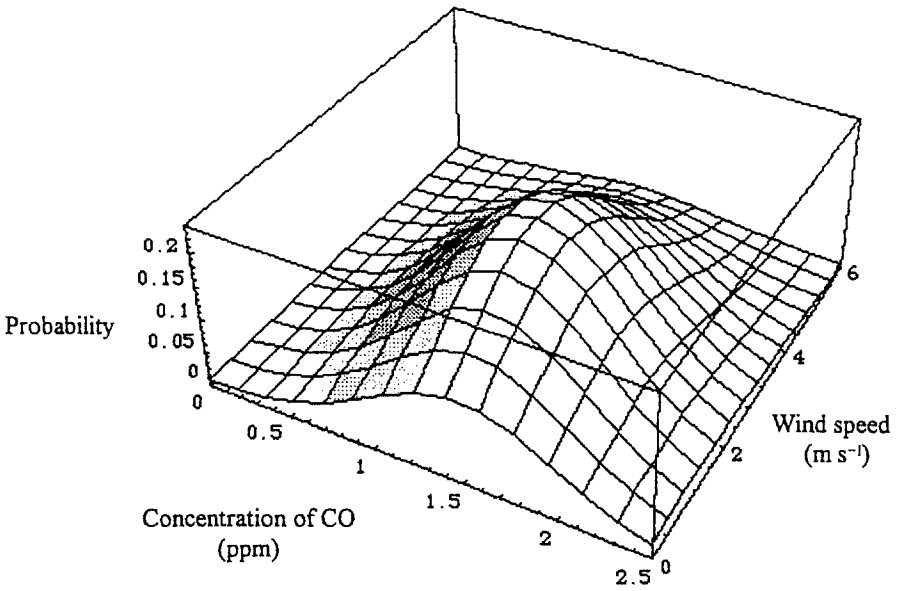


Fig. 12. Computed continuous normal probability distribution for CO concentrations.

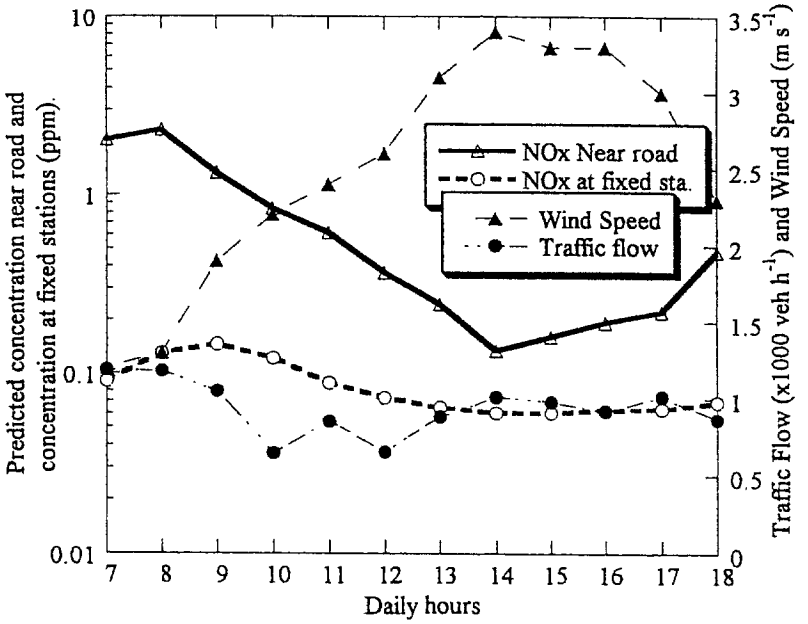


Fig. 13. Comparison of predicted road level $NO_x$ concentrations and concentrations measured at a local monitoring station.

2.5 and 3.0 m $s^{-1}$, the CRC/CMR values are 5 and 2 for $NO_x$ and CO, respectively. These findings indicate a critical level of wind speed (3 m $s^{-1}$) beyond which the ratios of concentration at different levels approach unity.

The differences between monitored and predicted concentrations should be, in part, due to the fact that the monitoring stations are elevated above the roadway. The ratio of $NO_x$ concentrations for elevated and ground-level receptors is higher than that for CO under all wind conditions. The difference is believed to be in part due to the fact that the $NO_x$ receptor is located higher above road level than the CO receptor.

The biggest differences between predicted and monitored CO concentrations are indicated in the morning, and the biggest differences for $NO_x$ are in the afternoon. It may be that temperature effects on emission rates are inadequately accounted for in the model. There are also a number of other theoretical or experimental factors that may contribute to these differences.

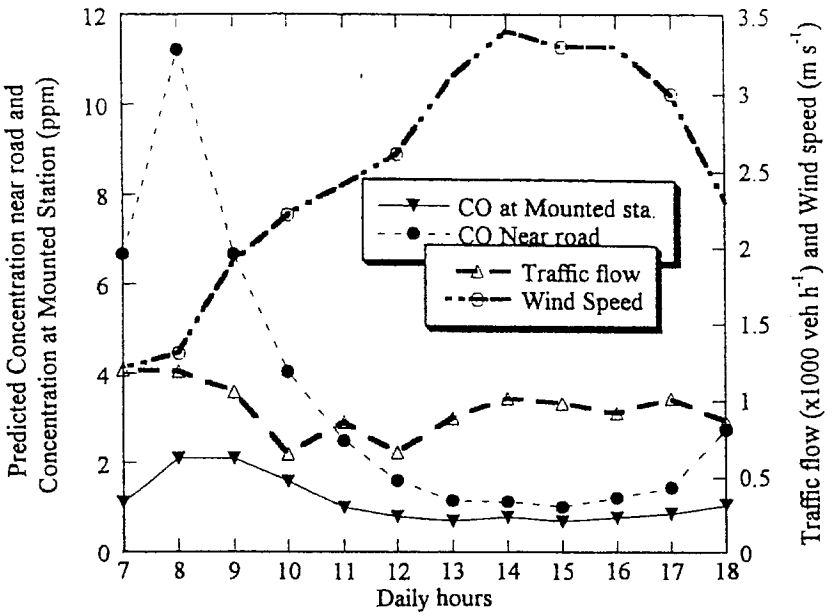


Fig. 14. Comparison of predicted road level CO concentrations and concentrations measured at a local monitoring station.

## 6. MODEL SENSITIVITY ANALYSIS

In order to establish the importance of individual parameters in the model, this section subjected the model to sensitivity analysis under wide range of conditions. Section 6.1 reports on the effects of vehicle dimensions to wind speed and dispersion parameters in microenvironments for various wind road angles and section 6.2 outlines wind speed on the downwash of pollutants concentration.

### *6.1. Vehicle dimensions to wind speed in microenvironments*

Since the model contains a number of stochastic parameters affecting the results and since the combination of any two variables with any of the others has a greater impact on the results, sensitivity analysis of the parameters has been carried out rather than concentrating on the final output. In most of the modeling technique vehicle dimensions are completely ignored in estimating wind speeds and dispersion parameter in microenvironments. This section presents the effects of vehicle dimensions on wind speed and dispersion parameter, varying wind road angle. Figures 15–21 present the effects of vehicle dimensions on wind speed in microenvironments for wind road angles of 10, 45, 90, 135, 225, 270, and 315°, respectively. For wind road angle 10°, there is not much variation of wind speed, and for wind road angles equal to and greater than 45°, marked variations are observed for larger vehicles; heavy duty trucks, buses, and special types of vehicles. For wind road angles 225, 270 and 315°, much variation in wind speed for all sizes of vehicles are observed.

After emission from vehicle tailpipes, pollutants blow due to their inertia. Transport, dispersion, and deposition cause the movements of pollutant in the atmosphere. Transport is a movement caused by a time-averaged wind flow. Dispersion results from ambient turbulence and turbulence induced by vehicles and also the horizontal advection due to heat generated from vehicles. Apart from natural transport and dispersion processes, moving vehicles themselves cause considerable mixing that influences pollutant concentrations within 100 m of a highway. The aerodynamic drag of a moving vehicle causes a turbulent wake in which pollutants initially mix. The size and speed of the vehicle influence this mixing and is most pronounced on concentration when the wind is nearly parallel to the axis of highway.

Dispersion due to vehicle induced turbulence is dependent on the cross-sectional areas of vehicles. Most of the dispersion models ignore the size of vehicles in estimating lateral and vertical dispersion lengths. In HIWAY 2 (Petersen, 1980) lateral and vertical dispersion lengths are estimated using some empirical relationships, irrespective of vehicle sizes. However, in this study we considered different sizes of Japanese vehicles to estimate the dispersion parameters. Figures 22

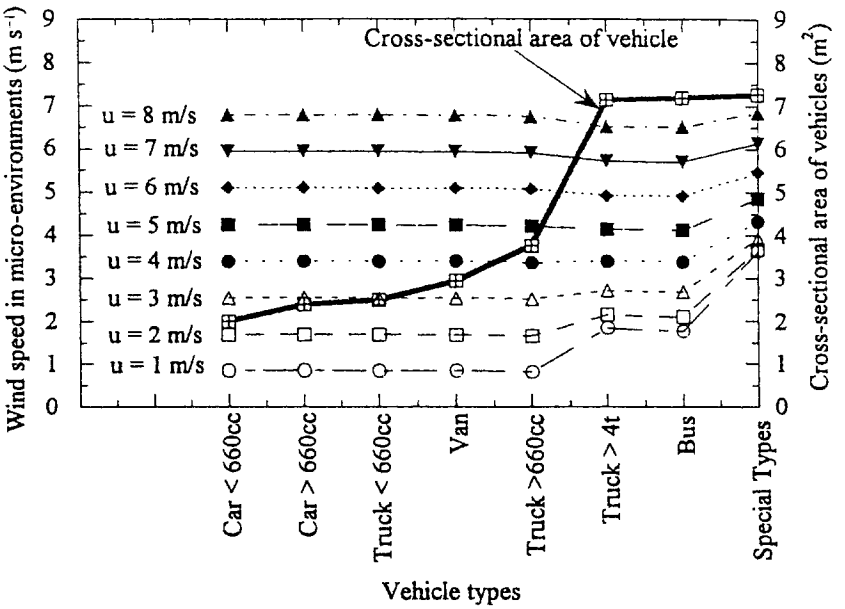


Fig. 15. Effects of vehicle dimensions on wind speed in microenvironments for wind-road angle, $\alpha = 10°$.

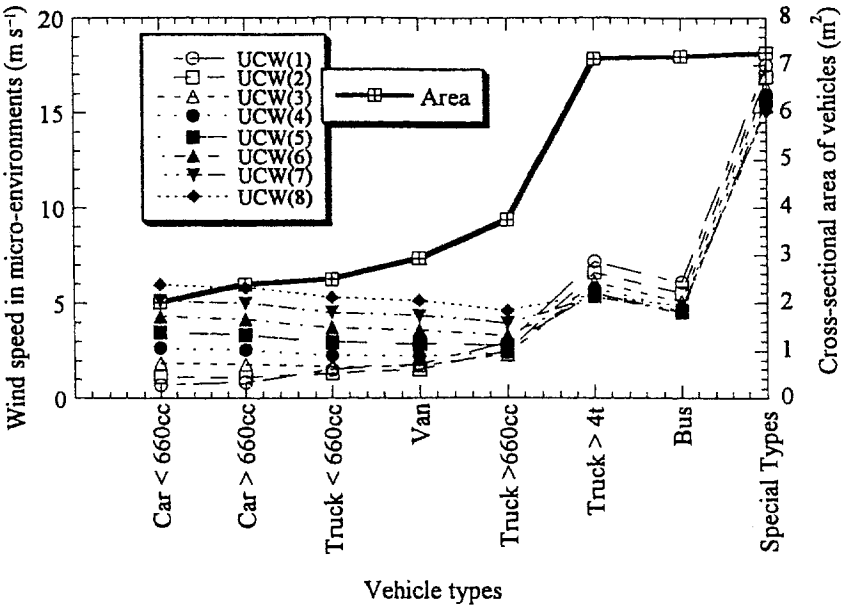


Fig. 16. Effects of vehicle dimensions on wind speed in microenvironments for wind-road angle, $\alpha = 45°$.

and 23 present the effects of vehicle dimensions on vertical and lateral dispersion parameters for various wind road angles. It is observed that dispersion parameters are directly related to vehicle dimensions. For larger vehicles lateral and vertical dispersion lengths are greater. For wind-road angles 45 and 225° lateral dispersion lengths are the largest, followed by 135 and 315° road angles, and almost parallel wind. For vertical wind (90 and 270°) lateral dispersion lengths are the least for smaller to larger vehicles. On the other hand, for vertical wind (90 and 270°) vertical dispersion is the highest, followed by the wind-road angles 45, 135, 225, and 315° and least for the parallel wind.

### *6.2. Wind speed to pollutant concentration*

A mathematical model has been established to indicate the stochastic situation in urban roads where street canyons restrict normal dispersion of pollutants. To have a clear perspective on results, generalized formulation of the model-output is given through a series of graphics from

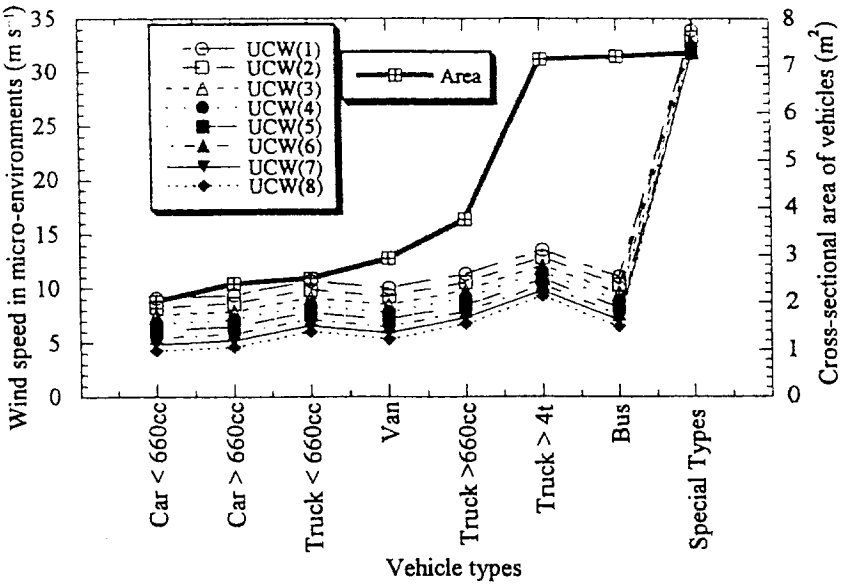


Fig. 17. Effects of vehicle dimensions on wind speed in microenvironments for wind-road angle, $\alpha = 90°$.

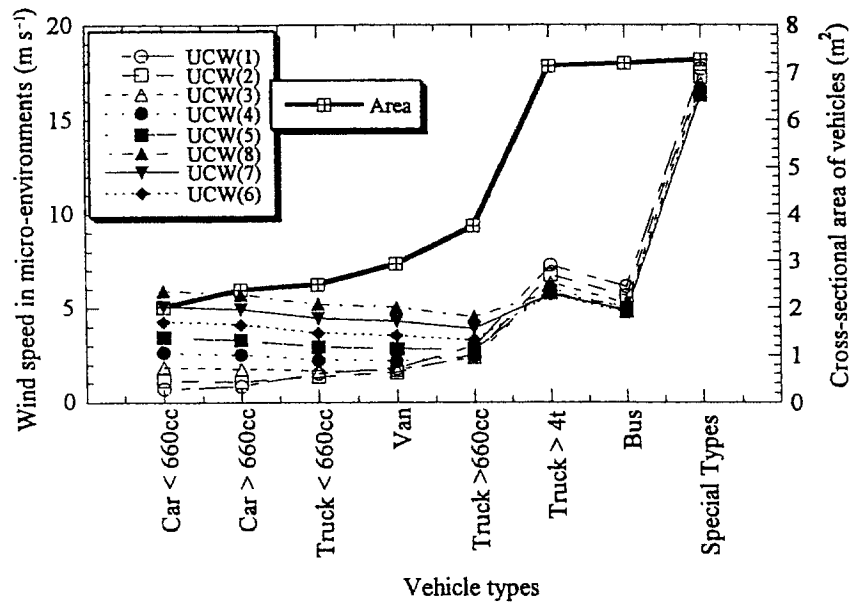


Fig. 18. Effects of vehicle dimensions on wind speed in microenvironments for wind-road angle, $\alpha = 135°$.

Figs 24–27. These figures are drawn by varying wind speed from 1 to 7 m $s^{-1}$ with an increment of 0.5 m $s^{-1}$. The model contains many variables affecting the results and the combination of every single variable with each of the four pollutants (CO, NO, $NO_2$, and $NO_x$) was thought to present an impractical task, the sensitivity analysis of wind on $NO_x$ has only been performed. Figures 24–27 show similar patterns for various wind conditions. Figures 24–27 outline that in two peak traffic periods (7–9 a.m. and 6–8 p.m.) on Japan's roads pollutant concentrations are higher. The notable factor to be considered is that for a small increment of wind velocity from 1 m $s^{-1}$, a larger contribution attributed. For wind velocity greater than or equal to 4 m $s^{-1}$, no further change in background concentration appeared even for the highest wind velocity 7 m $s^{-1}$, which indicates that meteorology could be to some extent, useful for the dilution of concentration.

Figures 24–27 represent that in two peak traffic periods (7–9 a.m. and 6–8 p.m.) on Japan's road pollutant concentrations are higher. For a smaller increase in wind speed from its lowest value

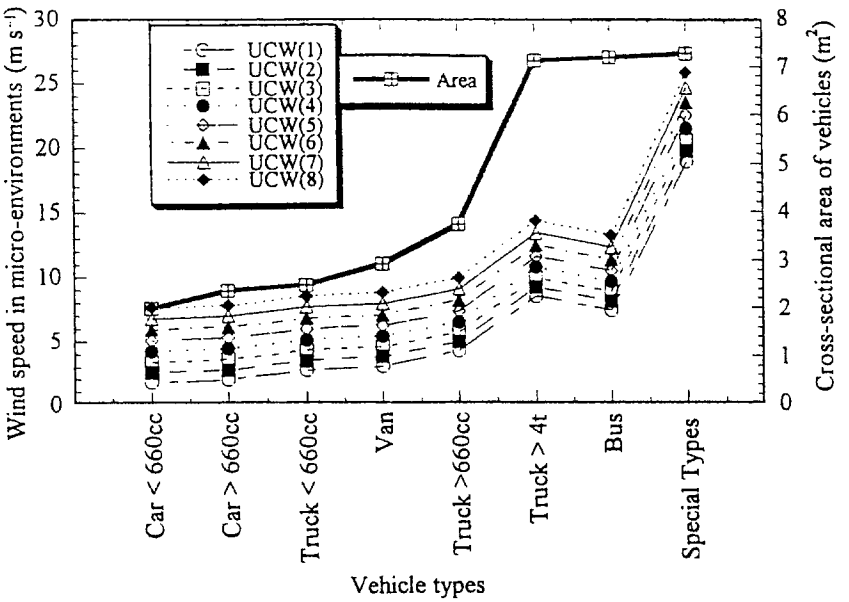


Fig. 19. Effects of vehicle dimensions on wind speed in microenvironments for wind-road angle, $\alpha = 225°$.

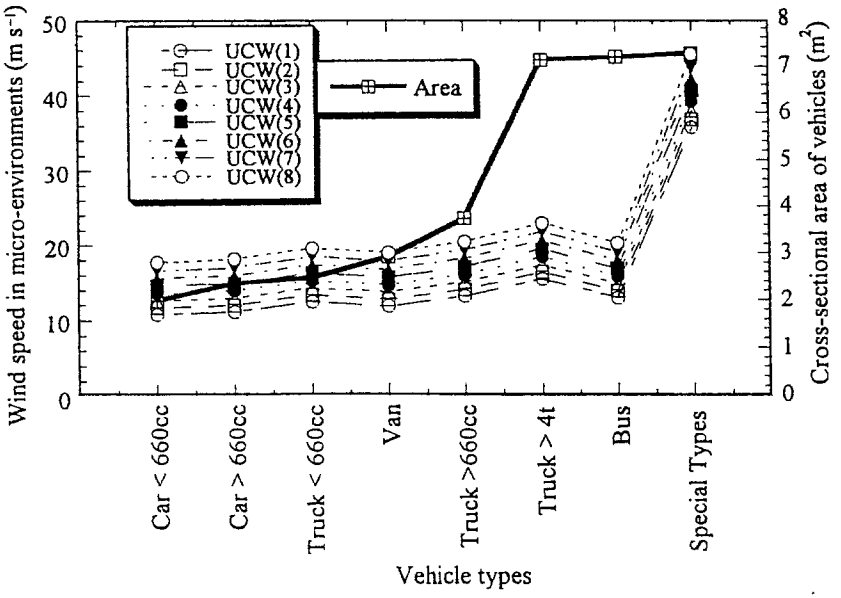


Fig. 20. Effects of vehicle dimensions on wind speed in microenvironments for wind-road angle, $\alpha = 270°$.

(1 m $s^{-1}$) there are marked variations of background pollutants concentration. To have a favourable perspective of the impact of wind, a percent variation of the decrease of background concentration from its initial value has been described in Figs 24–27. The graphics are drawn for a set of hourly variations of concentration that is being emitted directly from vehicles. For an increment of 0.5 m $s^{-1}$ of wind speed value a 45–50% pollutant is transferred in comparison to the lowest wind situation.

## 7. MODEL EVALUATION RESULTS

For the purpose of model evaluation concentrations of NO, $NO_2$, and $NO_x$ were monitored. Another experiment was performed to identify street-canyon effects on the distribution of wind and temperature. Some simplifications are done on the experimental data. The experimental road is east-west aligned, the receptors are located at the south of the road. For getting downwind pollutant concentration, northbound wind flow should be considered. But the monitoring data we

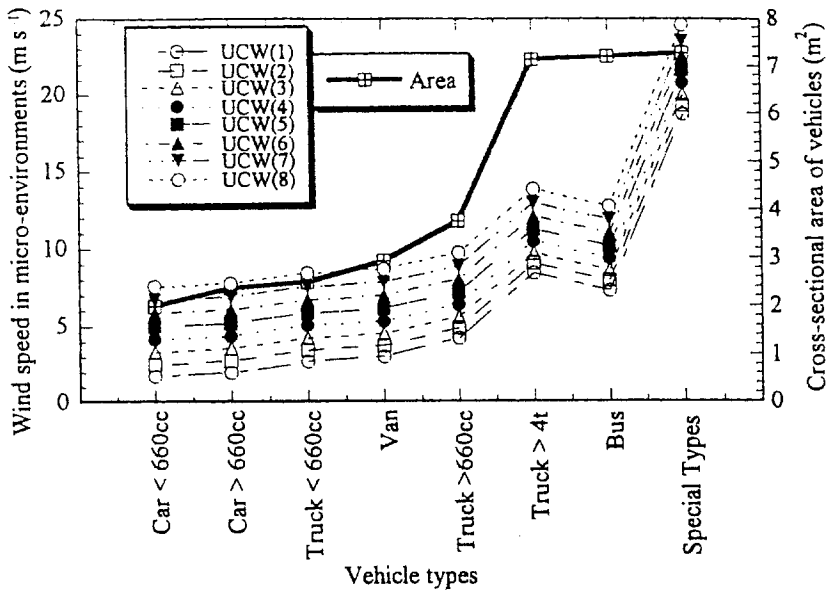


Fig. 21. Effects of vehicle dimensions on wind speed in microenvironments for wind-road angle, $\alpha = 315°$.

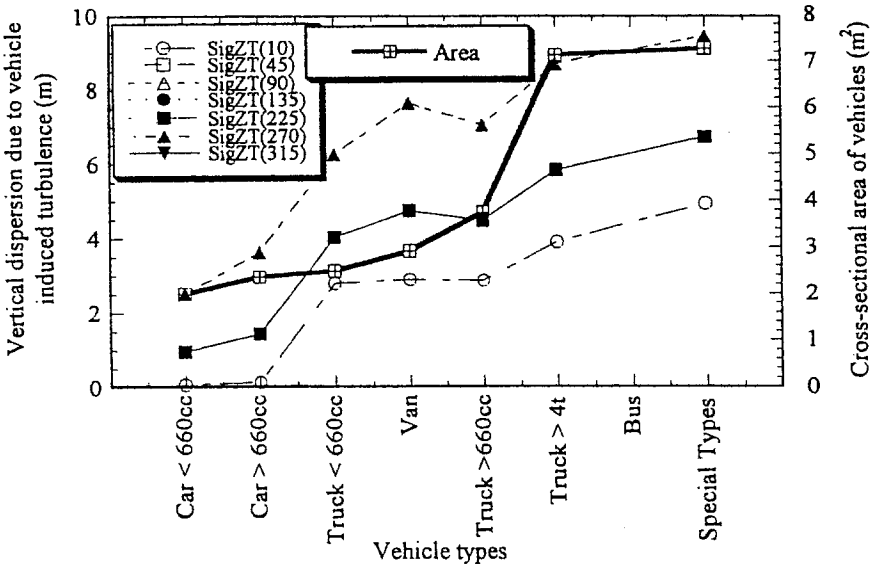


Fig. 22. Effects of vehicle dimensions on vertical dispersion parameter in microenvironments for various wind-road angle.

collected in our experiment was during the southbound wind. Hence, these data are to be considered as the background concentration, and in Part I, a theory has already been developed for the framework of background concentration. In the following sections experimental and prediction results are presented for the evaluation of the model.

*7.1. Wind distribution in canyon*

Wind speed plays a vital role in atmospheric dispersion. The variations of wind speed are presented in Fig. 28. Ambient wind, wind speed in street canyon, and wind speed in microenvironments (the combined effects of street-canyon and vehicle wake) are outlined in Fig. 28. Wind speed decreases with canyon depth and suddenly increases near the ground due to vehicle wake turbulence.

Comparison of the predicted wind speed in canyon with observed wind is presented in this section. Data are collected from 9 a.m. to 5 p.m. of a day at 10 min intervals, at the experimental site. The comparison is presented in Fig. 29. The relationship indicates that predicted and observed

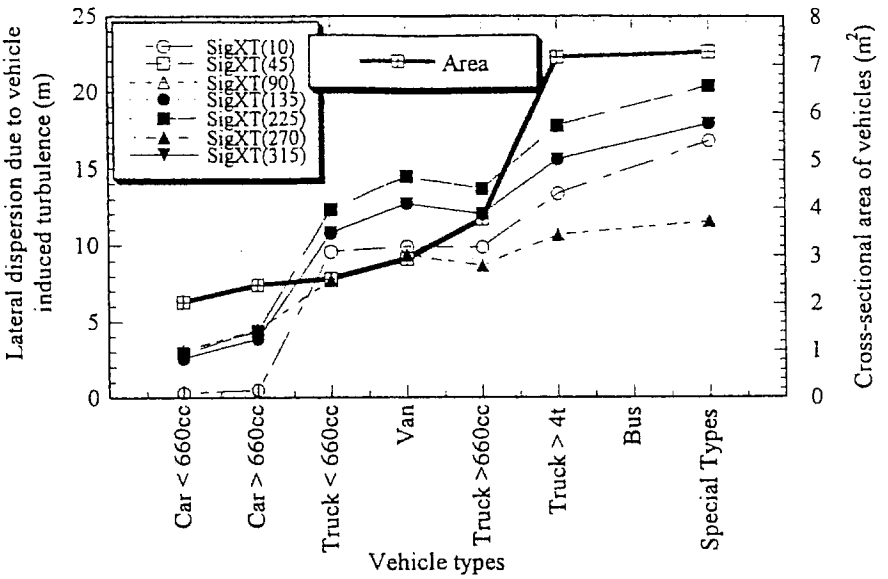


Fig. 23. Effects of vehicle dimensions on lateral dispersion parameter in microenvironments for various wind-road angle.

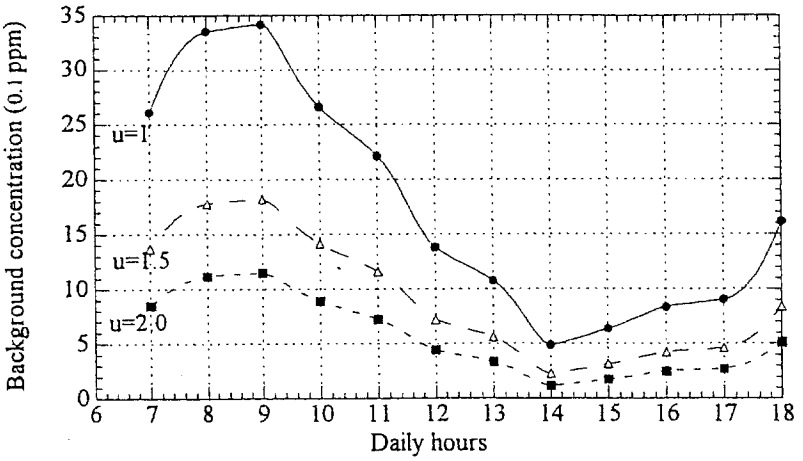


Fig. 24. Effects of wind speed on background concentration of $NO_x$ for u = 1, 1.5, and 2.0 m $s^{-1}$.

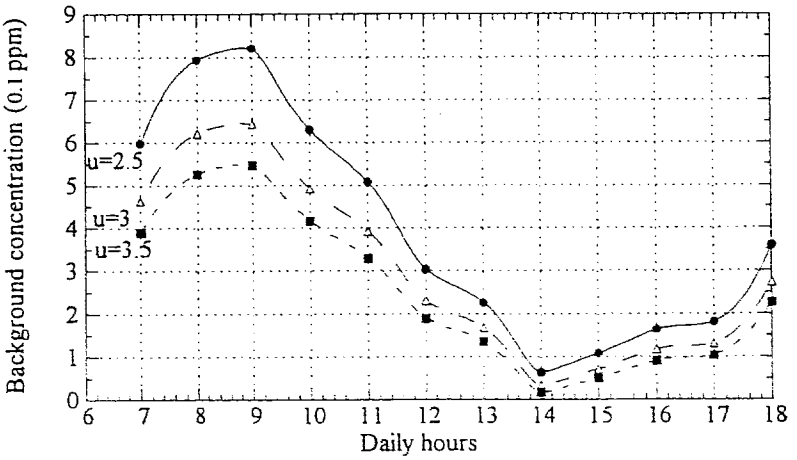


Fig. 25. Effects of wind speed on background concentration of $NO_x$ for u = 2.5, 3, and 3.5 m $s^{-1}$.

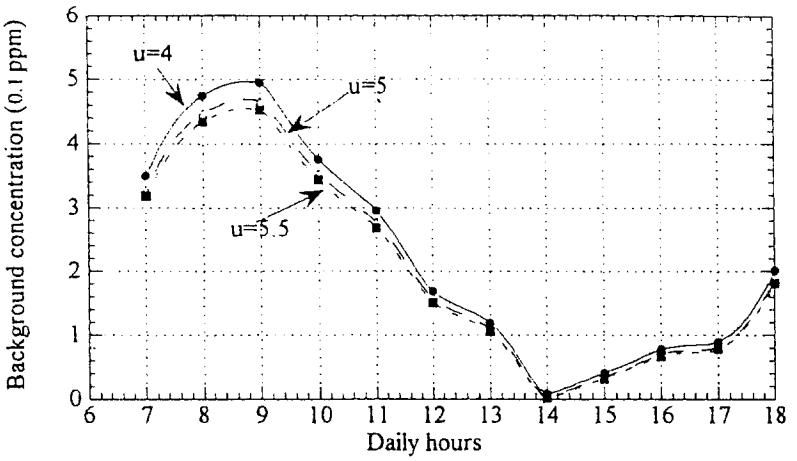


Fig. 26. Effects of wind speed on background concentration of $NO_x$ for u = 4, 5, and 5.5 m $s^{-1}$.

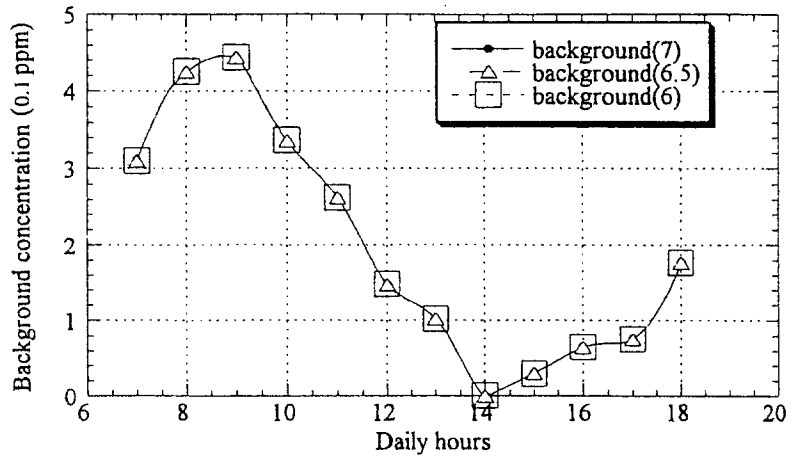


Fig. 27. Effects of wind speed on background concentration of $NO_x$ for u = 6, 6.5, and 7 m $s^{-1}$.

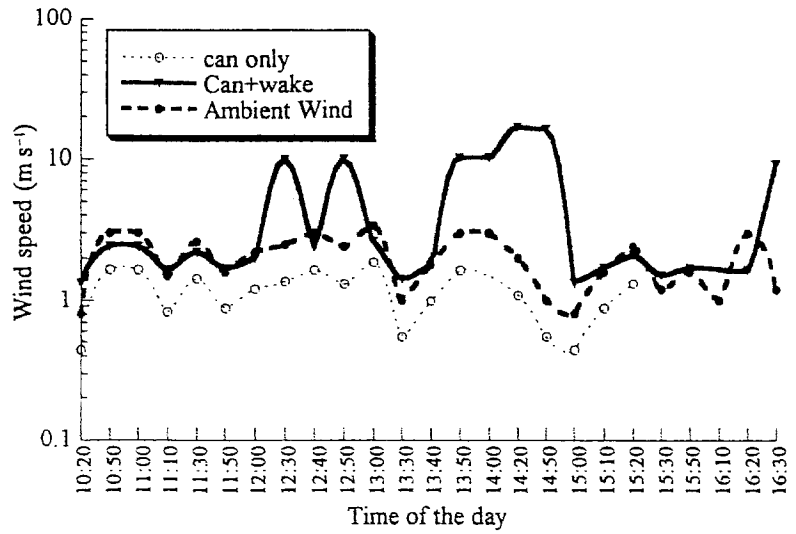


Fig. 28. Effects of different physical factors on wind speed.

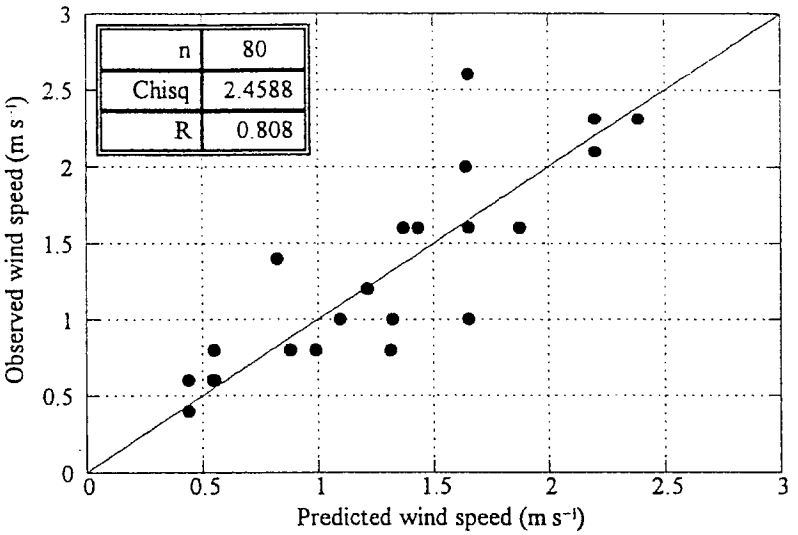


Fig. 29. Predicted versus observed wind in street canyon.

wind is fairly correlated and the coefficient of correlation is 0.808. The fluctuations are considered, in part, due to the fact that wind speed is somehow disturbed by the wake turbulence generated by vehicular traffic, and the wind fluctuations occur due to the reflection from the buildings, though the wind sensor was at height of 1 m from the ground and 7.5 m away from the road.

*7.2. Dispersion parameter*

For wind parallel to traffic flow, lateral dispersion occurs due to traffic movements. The ratio between total dispersion for traffic induced turbulence and ambient turbulence is less than or equal to 10 (Sedefian *et al.*, (1981)). For wind directions perpendicular to the traffic direction, total diffusivity is dependent on wind speed and the ratio lies somewhere between 2 and 25 (Sedefian *et al.*, 1981). Figure 30 presents the relationship between horizontal and vertical dispersion parameters due to three physical attributes. A typical relationship is outlined in Fig. 30, which approximates the ratio between lateral and vertical dispersion around 2. Based on this ratio, a straight line is drawn which provides a correlation coefficient equal to 0.69.

*7.3. Pollutant concentrations*

The complexity of the flow within the urban canyon, particularly in road microenvironments, and the paucity of full-scale experimental data have perhaps hindered the development and

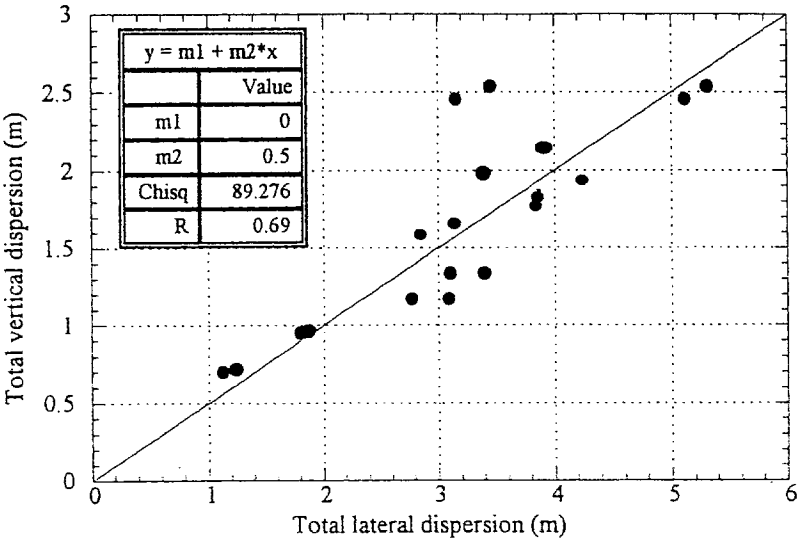


Fig. 30. Relationship between total lateral dispersion and vertical dispersion.

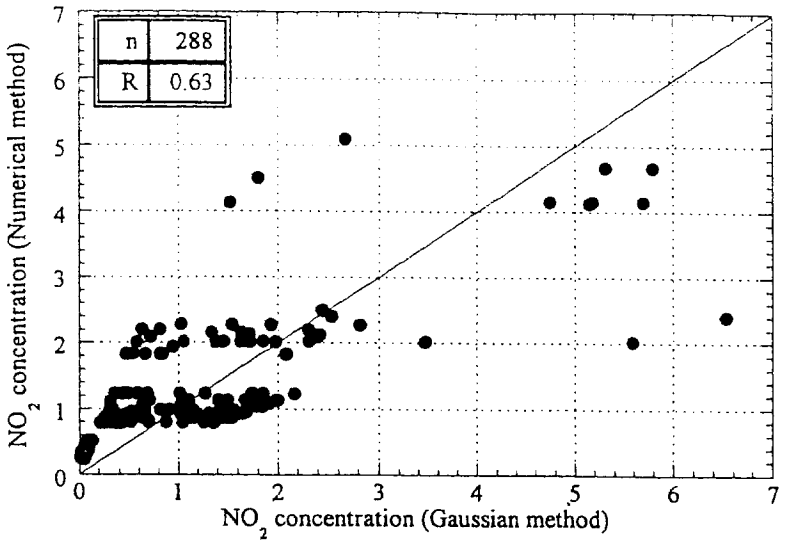


Fig. 31. $NO_2$ concentration relation between numerical and Gaussian method.

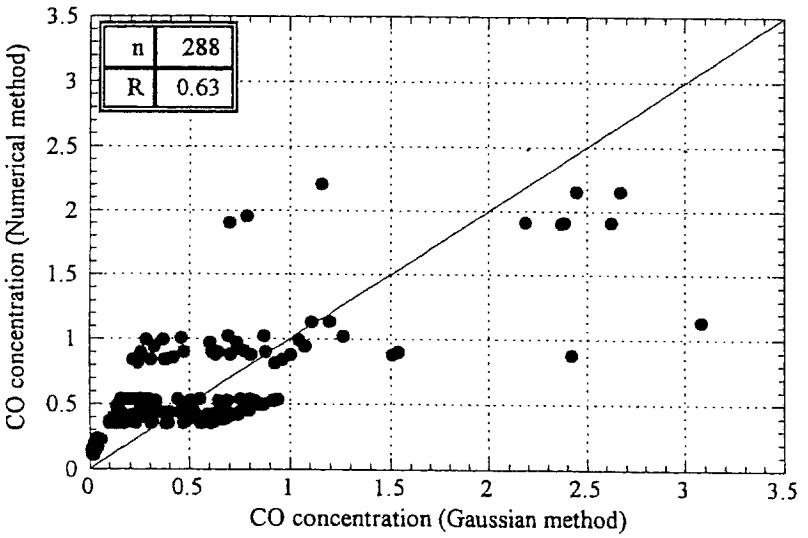


Fig. 32. CO concentration relation between numerical and Gaussian method.

proliferation of models applicable to the urban canyon microenvironment. In Part I, a modified Gaussian equation and a numerical method have been introduced. Both predict active pollutant concentration. The scatter plots of the Gaussian vs numerical methods are presented in Figs 31 and 32 for $NO_2$ and CO, respectively. Figure 31 presents the relationship between $NO_2$ concentration estimated using Gaussian and numerical methods. The concentration obtained by numerical method is considerably less than that obtained by Gaussian method. This indicates that the numerical method predicts too large a volume occupied by the pollutants and the downwind distance traveled by the gas particles is considered inaccurate.

In the region of initial dispersion, the pollutant is more influenced by local traffic-produced turbulence than by the prevailing wind, so some of the pollutant is dispersed in an upwind direction. The rate of fall of concentration is, however, much greater than in the downwind direction. This is simulated in the model by calculating the concentration at points upwind of the source as if they were downwind but at a greater distance away. In Part I theories are established to identify the pollutant concentration buildup and background pollutant concentration. Figures 33–35 present the prediction and experimental results. Though microscale analysis is normally done in highway projects for CO concentration, however, due to the lack of CO data we carried out analysis on NO, $NO_2$, and $NO_x$. Figure 33 depicts predicted vs experimental data for NO concentration. The experiment was performed for a period of one month, and traffic data (census) was

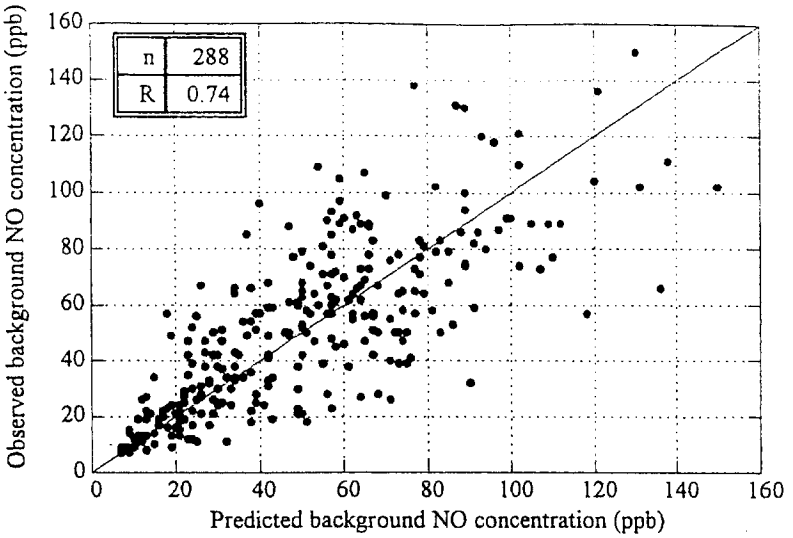


Fig. 33. Predicted vs measured NO concentration in urban road microenvironments.

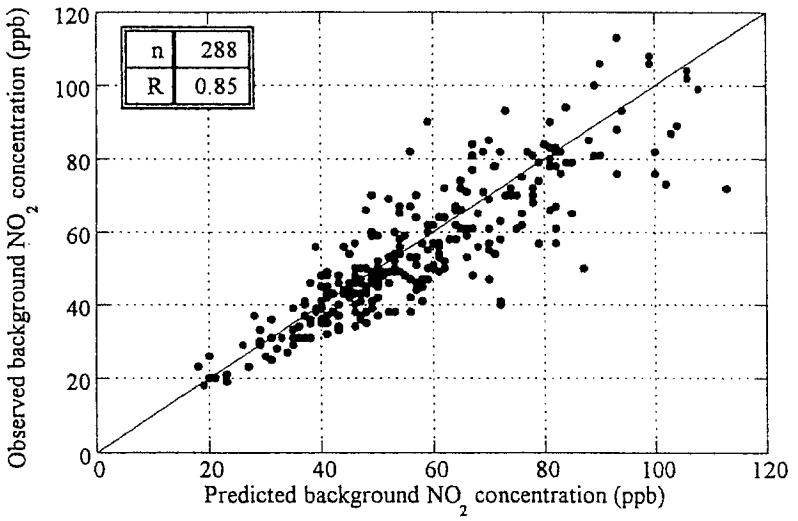


Fig. 34. Predicted vs measured $NO_2$ concentration in urban road microenvironments.

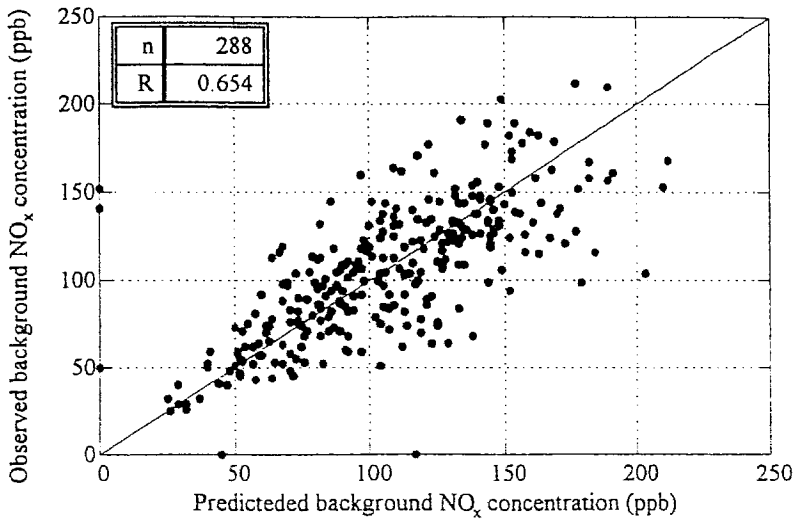


Fig. 35. Predicted vs measured $NO_x$ concentration in urban road microenvironments.

only available for 7 a.m. to 6 p.m., and for comparisons of traffic flows, only weekdays data are taken into consideration for the computer simulation. From the point of evaluation it can be concluded that theory predicts microenvironmental concentration of NO, $NO_2$, and $NO_x$ accurately. The closest agreement between prediction and observed results found is for $NO_2$ concentration (Fig. 34).

## 8. CONCLUSIONS

Simple models for the flow, turbulence, dispersion, and pollutants concentrations within canyon microenvironments have been developed in Part I and this paper analyzes and evaluates the modeling results. Analysis performed on a database of Nagoya City taken for a period of 24 days for 12 h a day indicate that:

- wind velocity reduces in the canyon
- wind velocity suddenly increases near the ground due to vehicle wake turbulence
- relationship between lateral and vertical dispersion of pollutants fairly correlates with the description provided in the literature
- wind and other meteorology substantially dominates the flow pattern in street canyon
- in predicting pollutant concentration, numerical method underestimates than the Gaussian method
- predicted and observed newly defined background concentrations correlate fairly with each other.

*Acknowledgements*—The Ministry of Education, Science and Culture (MONBUSHO), Japan provided funds for the development and evaluation of this model. The authors wish to confer their thanks to Nagoya City Environmental Science Research Institute for providing model evaluation data. Sincere thanks are due to Mr Md. Mosaddeq-ur Rahman, Nagoya Institute of Technology for his help in the experimental work. The authors express their sincere appreciation to the reviewers for suggested improvements to the papers.

## REFERENCES

Benson, P. E. (1989) CALINE4—a dispersion model for predicting air pollution concentrations near roadways (revised), FHWA/CA/TL-85/1.

Chock, D. P. (1978) A simple line-source model for dispersion near roadways. *Atmospheric Environment* **12**, 823.

Eskridge, R. E. and Hunt, J. C. R. (1979) Highway modeling: Part 1: prediction of velocity and turbulence fields in the wake of vehicles. *J. Appl. Meteorol* **18**, 387–400.

Karim, M. M. (1997) Modeling and control of traffic pollution in urban road-microenvironments. Doctoral dissertation, Department of Civil Engineering, Nagoya Institute of Technology, Nagoya, Japan.

Karim, M. M. and Matsui, H., (1998) A mathematical model of wind flow, vehicle wake, and pollutant concentration in urban road microenvironments—I: model description, *Transportation Research D* **3**(2), 81–92.

Karim, M. M. and Matsui, H., (1994), A stochastic model of emission expansion for an urban road. In *Proceedings of 5th Vehicle Navigation & Information Systems Conference*, August 31 –September 2, IEEE 94CH35703, IEEE, Yokohama, Japan, pp. 363–368.

Karim, M. M., and Matsui, H., (1995) Effects of wind speed on the dispersion of pollutant concentration in a road of nagoya city. In *Proceedings of Fourth International conference in Urban Planning and Urban Management*. July 11–14, Department of Geography and Environmental Studies. Melbourne University, Melbourne, Australia. pp. 189–199.

Lloyd, E. (1980) *Handbook of Applicable Mathematics, Volume II: Probability*, John Wiley & Sons, Chichester.

Petersen, W. B. (1980) *User's Guide for HIWAY-2, A Highway Air Pollution Model*, EPA-600/8-80-018 or PB 80-227556.

Sedefian, L., Rao, S. T. and Czapski, U. (1981) Effects of traffic-generated turbulence on near field dispersion. *Atmospheric Environment* **15**, 527.

Tong, Y. L. (1990) *The Multivariate Normal Distribution*. Springer-Verlag. New York.

Yamartino, J. R. and Wiegand, G. (1986) Development and evaluation of simple models for the flow, turbulence and pollutant concentration fields within an urban street canyon. *Atmospheric Environment* **20**(11), 2137.